Interaction of gravitational waves with strongly magnetized plasmas

Heinz Isliker,[1,*] Ingmar Sandberg,[2] and Loukas Vlahos[1]

[1]*Section of Astrophysics, Astronomy and Mechanics, Department of Physics, University of Thessaloniki, GR 541 24 Thessaloniki, Greece*

[2]*Department of Electrical and Computer Engineering, National Technical University of Athens, GR 157 73 Athens, Greece*

(Received 26 September 2005; revised manuscript received 17 July 2006; published 3 November 2006)

We study the interaction of a gravitational wave (GW) with a plasma that is strongly magnetized. The GW is considered a small disturbance, and the plasma is modeled by the general relativistic analogue of the induction equation of ideal MHD and the single fluid equations. The equations are specified to two different cases, first to Cartesian coordinates and a constant background magnetic fields, and second to spherical coordinates together with a background magnetic field that decays with the inverse radial distance. The equations are derived without neglecting any of the nonlinear interaction terms, and the nonlinear equations are integrated numerically. We find that for strong magnetic fields of the order of 10^{15} G the GW excites electromagnetic plasma waves very close to the magnetosonic mode. The magnetic and electric field oscillations have very high amplitude, and a large amount of energy is absorbed from the GW by the electromagnetic oscillations, of the order of 10^{23} erg/cm^3 in the case presented here, which, when assuming a relatively small volume in a star's magnetosphere as an interaction region, can yield a total energy of at least 10^{41} erg and may be up to 10^{43} erg. The absorbed energy is proportional to B_0^2, with B_0 the background magnetic field. The energizing of the plasma takes place on fast time scales of the order of milliseconds. Our results imply that the GW-plasma interaction is an efficient and important mechanism in magnetar atmospheres, most prominently close to the star, and, under very favorable conditions though, it might even be the primary energizing mechanism behind giant flares.

DOI: 10.1103/PhysRevD.74.104009 PACS numbers: 04.30.Nk, 04.25.Dm, 52.35.Mw, 95.30.Sf

I. INTRODUCTION

Gravitational waves (GW) can carry a large amount of energy near the sources where they are generated (e.g. [1]). They tend not to interact much with matter under normal conditions; it has been shown though in a number of articles (e.g. [2–10]) that GWs excite various kinds of plasma waves, the more efficient, the stronger the background magnetic field is and the more tenuous the plasma is. Most of these studies are analytical and the equations describing the GW-plasma interaction were linearized, only Ref. [4] made an analytical study of a nonlinear model, Refs. [2,5] took some second order effects into account, and Ref. [11] performed a numerical study. The GW-plasma interaction is a totally nonlinear effect, and there is so far no conclusive answer to the question of how much energy can be absorbed by a plasma from a GW.

Here, we study the GW-plasma interaction in its full nonlinearity, solving the nonlinear system of equations numerically. Our main interest is in the amount of energy absorbed by the plasma from the GW and in the kind of plasma waves excited by the GW, and we focus on the case of very strong magnetic fields of the order of 10^{15} G.

Our results show that the interaction of gravitational waves with plasmas is very efficient in transferring energy from the GW to the plasma if the magnetic field is very strong, of the order of 10^{15} G. Magnetic fields of this strength are known to be realized at the surface of magnetars, which are strongly magnetized neutron stars (see e.g. [12]) that at the same time appear as soft gamma ray repeaters (SGR). We will address the question whether the GW-plasma interaction might be the primary mechanism behind giant flares on magnetars (highly energetic outbursts in the stars' magnetospheres; see e.g. [13]). We will also discuss whether the GW-plasma interaction can provide the energies observed in short gamma ray bursts (GRB; see e.g. [14]), so that short GRBs could be interpreted as giant flares on magnetars that carry even more energy than the giant flares observed so far. A related model of short GRBs as giant flares on magnetars is discussed e.g. in [15–17]), where the giant flares are caused though by a catastrophic reconfiguration of the stellar magnetic field, and not by the GW-plasma interaction as we will discuss it here. The origin of short GRBs is far less established than that of the long GRBs. The energy released in short GRBs is currently estimated to be at least 10^{48} erg [16]; the uncertainty is mainly due to the problem of associating short GRBs with physical objects. The duration of short GRBs is less than 2 seconds. Giant flares have similar durations and release energies in the range 10^{44} to 10^{46} erg (e.g. [13]).

In Sec. II, we introduce the basic equations and specify the one-dimensional model. A linear analysis of the equations is given in Sec. III. In Sec. IV, the results from the numerical solution of the nonlinear equations are presented, for the case of a constant background magnetic field. In Sec. V, we transform the system of equations to spherical coordinates, and we solve them along the radial direction, for the case of a background magnetic field that decays with the inverse distance from the central star.

*Electronic address: isliker@helios.astro.auth.gr

Section VI discusses the application of our findings to magnetar atmospheres, and Sec. VII contains the conclusions.

II. BASIC EQUATIONS

The GW is considered as a small amplitude perturbation of the otherwise flat spacetime, and we assume it to be + polarized and to propagate along the z-direction, so that the metric has the form

$$g_{ab} = \mathrm{diag}(-1, 1 + h, 1 - h, 1), \tag{1}$$

with $h(z, t) \ll 1$ the amplitude of the GW [18]. Our aim is to express the final equations in terms of the potentially observable quantities (electric field $\vec{E}$, magnetic field $\vec{B}$, 3-velocity $\vec{V}$ of the fluid, and rest-mass density ρ), which can either be defined in a local inertial frame (LIF) or in an orthonormal (ON) frame (ONF) [18]. Here, we use the ONF, because it is a global frame, and it can be shown that the ONF in our case is locally equivalent to a LIF when applying the particular coordinate transformation given in [19]. Indices of quantities in the ONF carry a hat in the following. The transformation from and to the ONF is given by the transformation matrix

$$(\mathbf{e}_{\hat{a}})^b = \mathrm{diag}\left(1, \frac{1}{\sqrt{1+h}}, \frac{1}{\sqrt{1-h}}, 1\right) \tag{2}$$

and its inverse $(\mathbf{e}^{\hat{a}})_b$. Here, $\mathbf{e}_{\hat{a}}$ are the ON basis vectors, and $(\mathbf{e}_{\hat{a}})^b$ are their coordinates in the coordinate base. The metric in the ONF is of flat spacetime form, $\eta_{\hat{a}\hat{b}} = \mathrm{diag}(-1, 1, 1, 1)$. In the ONF, 4-vectors and tensors take the same form as in flat spacetime, the effects of curvature appear only through the covariant derivatives.

The covariant derivatives in the ONF are denoted by ";" and defined as, e.g. in the case of a 4-vector u^a,

$$u^{\hat{a}}{}_{;\hat{c}} = (\mathbf{e}_{\hat{c}})^k u^{\hat{a}}{}_{,k} + \gamma^{\hat{a}}{}_{\hat{b}\,\hat{c}} u^{\hat{b}}, \tag{3}$$

where "," denotes partial derivatives, and where the

$$\gamma^{\hat{a}}{}_{\hat{b}\,\hat{c}} := (\mathbf{e}_{\hat{b}})^i{}_{;k} (\mathbf{e}^{\hat{a}})_i (\mathbf{e}_{\hat{c}})^k \tag{4}$$

are the Ricci rotation coefficients [19]. For the metric g_{ab} and our choice of ON base vectors, the Ricci rotation coefficients found to be nonzero are

$$\gamma^{\hat{x}}{}_{\hat{z}\,\hat{x}} = \frac{1}{2}\partial_z h \frac{1}{1+h} \tag{5}$$

$$\gamma^{\hat{x}}{}_{\hat{t}\,\hat{x}} = \frac{1}{2c}\partial_t h \frac{1}{1+h} \tag{6}$$

$$\gamma^{\hat{y}}{}_{\hat{z}\,\hat{y}} = -\frac{1}{2}\partial_z h \frac{1}{1-h} \tag{7}$$

$$\gamma^{\hat{y}}{}_{\hat{t}\,\hat{y}} = -\frac{1}{2c}\partial_t h \frac{1}{1-h} \tag{8}$$

$$\gamma^{\hat{z}}{}_{\hat{x}\,\hat{x}} = -\frac{1}{2}\partial_z h \frac{1}{1+h} \tag{9}$$

$$\gamma^{\hat{z}}{}_{\hat{y}\,\hat{y}} = \frac{1}{2}\partial_z h \frac{1}{1-h} \tag{10}$$

$$\gamma^{\hat{t}}{}_{\hat{x}\,\hat{x}} = \frac{1}{2c}\partial_t h \frac{1}{1+h} \tag{11}$$

$$\gamma^{\hat{t}}{}_{\hat{y}\,\hat{y}} = -\frac{1}{2c}\partial_t h \frac{1}{1-h}. \tag{12}$$

We assume an ideal conducting fluid, so that the electric field is given by the ideal Ohm's law,

$$0 = F^{\hat{a}\,\hat{b}} u_{\hat{b}}/c, \tag{13}$$

which in the ONF takes the usual form,

$$0 = \hat{\gamma}\left(\vec{E} + \frac{1}{c}\vec{V} \times \vec{B}\right), \tag{14}$$

with $\hat{\gamma} = 1/\sqrt{1 - \vec{V}^2/c^2}$, $u^{\hat{a}}$ the 4-velocity, $u^{\hat{a}} = \hat{\gamma}(c, V_x, V_y, V_z)$, and c the speed of light, and $F^{\hat{a}\,\hat{b}}$ Faraday's field tensor,

$$F^{\hat{a}\,\hat{b}} = \begin{pmatrix} 0 & E_x & E_y & E_z \\ -E_x & 0 & B_z & -B_y \\ -E_y & -B_z & 0 & B_x \\ -E_z & B_y & -B_x & 0 \end{pmatrix}. \tag{15}$$

The evolution of the magnetic field is determined by the Maxwell's equation [19]

$$F_{\hat{a}\,\hat{b};\hat{c}} + F_{\hat{b}\,\hat{c};\hat{a}} + F_{\hat{c}\,\hat{a};\hat{b}} = 0. \tag{16}$$

The electromagnetic (EM) energy momentum tensor is defined as

$$T^{\hat{a}\,\hat{b}}_{(\mathrm{EM})} = \frac{c^2}{4\pi}\left(F^{\hat{a}\,\hat{c}} F^{\hat{b}}_{\hat{c}} - \frac{1}{4}\eta^{\hat{a}\,\hat{b}} F^{\hat{c}\,\hat{d}} F_{\hat{c}\,\hat{d}}\right), \tag{17}$$

and for the fluid, we have the energy momentum tensor

$$T^{\hat{a}\,\hat{b}}_{(\mathrm{fl})} = H u^{\hat{a}} u^{\hat{b}} + \eta^{\hat{a}\,\hat{b}} p c^2, \tag{18}$$

where H is the enthalpy and p the pressure [19]. We assume an ideal and adiabatic fluid, so that

$$H = \rho c^2 + \frac{p}{\Gamma - 1} + p, \tag{19}$$

with Γ the adiabatic index. The total energy momentum tensor $T^{\hat{a}\,\hat{b}} = T^{\hat{a}\,\hat{b}}_{(\mathrm{fl})} + T^{\hat{a}\,\hat{b}}_{(\mathrm{EM})}$ yields the momentum and energy equations [19]

$$T^{\hat{a}\,\hat{b}}{}_{;\hat{b}} = 0. \tag{20}$$

Continuity is expressed by

$$(\rho u^{\hat{a}})_{;\hat{a}} = 0. \tag{21}$$

The evolution of the GW is determined by the linearized Einstein equation, where we take the backreaction of the plasma onto the GW into account:

$$-\partial_{tt}h + c^2\vec{\nabla}^2 h = -\frac{1}{2}\frac{16\pi G}{c^4}(\delta T_{xx} - \delta T_{yy}), \quad (22)$$

where δT_{xx}, δT_{yy} are the nonbackground, fluctuating parts of the components T_{xx}, T_{yy} of the total energy momentum tensor, and G is the gravitational constant [18]. To close the system of equations, we assume an adiabatic and isentropic equation of state,

$$p = K\rho^{\Gamma}. \quad (23)$$

The constant K is determined by assuming an ideal gas law for the constant background density ρ_0, i.e. $p_0 = \rho_0(k_B/m)T_0$, so that, on combining with Eq. (23), $K = \rho_0^{1-\Gamma}\frac{k_B}{m}T_0$, with T_0 the temperature.

A. The model

We focus on the excitation of MHD modes which propagate in the z-direction, parallel to the propagation direction of the GW and perpendicular to the background magnetic field $\vec{B}_0 = B_0\mathbf{e}_{\hat{x}}$. We let consequently $\vec{B} \parallel \mathbf{e}_{\hat{x}}$, $\vec{E} \parallel \mathbf{e}_{\hat{y}}$, and $\vec{V} \parallel \mathbf{e}_{\hat{z}}$, and all variables depend spatially only on z (note that B_x in the following is the total magnetic field—it includes B_0). In specifying the general equations to this particular geometry, (i) we express all 4-vector and tensor components through the potentially observable B_x, V_z, and ρ; (ii) we expand the covariant derivatives; (iii) we keep all nonlinear terms, no approximations are thus made (except for the linearized Einstein equation). In this way, we are led to a system of nonlinear, coupled, partial differential equations in a spatially 1D geometry: With the electric field E_y from Ohm's law [Eq. (14)],

$$E_y = -\frac{1}{c}V_z B_x, \quad (24)$$

Faraday's equation [Eq. (16)] is fully expanded to

$$\partial_t B_x = c\partial_z E_y + \frac{1}{2}B_x\frac{\partial_t h}{1-h} - \frac{1}{2}cE_y\frac{\partial_z h}{1-h}. \quad (25)$$

Expansion of the z-component of the momentum equation [Eq. (20)] yields

$$\begin{aligned}\partial_t q_{\hat{z}} + \partial_z\left[\left(q_{\hat{z}} - \frac{c}{4\pi}(-E_yB_x)\right)V_z\right] + \partial_z\left[\frac{c^2}{8\pi}(B_x^2 + E_y^2)\right] \\ + c^2\partial_z p + \frac{c}{8\pi}B_x(cB_x + E_yV_z)\frac{\partial_z h}{(1+h)} \\ - \frac{c}{8\pi}E_y(cE_y + B_xV_z)\frac{\partial_z h}{(1-h)} \\ - q_{\hat{z}}(\partial_t h + V_z\partial_z h)\frac{h}{1-h^2} = 0, \quad (26)\end{aligned}$$

where we defined the new momentum variable $q_{\hat{z}}$ as

$$q_{\hat{z}} := HV_z\hat{\gamma}^2 + \frac{c}{4\pi}(-E_yB_x). \quad (27)$$

The continuity equation [Eq. (21)] takes the form

$$\partial_t D + \partial_z(DV_z) - (D\partial_t h + DV_z\partial_z h)\frac{h}{1-h^2} = 0, \quad (28)$$

with the new density variable $D := \hat{\gamma}\rho$. The GW evolves according to

$$\partial_{tt}h = c^2\partial_{zz}h + \frac{2G}{c^2}(E_y^2 - (B_x^2 - B_0^2)) + \frac{16\pi G}{c^2}(p - p_0)h \quad (29)$$

[see Eq. (22)], where the background magnetic field B_0 and background pressure $p_0 = K\rho_0^{\Gamma}$ have been subtracted.

For the numerical solution, Eq. (29) has to be turned to first order in time, which is achieved by defining two new variables $a := \partial_t h$ and $b := c\partial_z h$, so that Eq. (29) is replaced by

$$\partial_t h = a, \quad (30)$$

$$\partial_t a = c\partial_z b + + \frac{2G}{c^2}(E_y^2 - (B_x^2 - B_0^2)) + \frac{16\pi G}{c^2}(p - p_0)h, \quad (31)$$

$$\partial_t b = c\partial_z a. \quad (32)$$

To recover $\hat{\gamma}$, ρ, p, H, and V_z from the explicitly evolving variables $q_{\hat{z}}$, D, and B_y, we solve the definition of $q_{\hat{z}}$ for V_z and insert it into a reformulated definition of $\hat{\gamma}$, which yields

$$(\hat{\gamma}^2 - 1)\left(H\hat{\gamma}^2 + \frac{1}{4\pi}B_x^2\right)^2 - \left(\frac{\hat{\gamma}q_z}{c}\right)^2 = 0, \quad (33)$$

where in the enthalpy H we replace ρ by $D/\hat{\gamma}$. Equation (33) is a nonlinear equation for $\hat{\gamma}$, which we solve numerically. Once $\hat{\gamma}$ is recovered, all the other primary variables follow in a straightforward way.

III. LINEAR ANALYSIS

Assuming perturbations of the form $\exp(-i\omega t + ik_z z)$, we linearize the one-dimensional momentum equation (26), and, on inserting the expressions for h, H, B_x, E_y, ρ, P as determined from the linearization of the Eqs. (19), (23)–(25), (28), and (29), we are led to the dispersion relation,

$$\begin{aligned}\left(\frac{\omega}{k_z}\right)^2\left(\rho_0c^2 + \frac{\Gamma P_0}{\Gamma - 1} + \frac{B_0^2}{4\pi}\right) \\ - \frac{c^2B_0^2}{4\pi}\left(1 + \frac{2g^2}{\omega^2 - \omega_{gw}^2 - g^2}\right) - c^2c_s^2\rho_0 = 0, \quad (34)\end{aligned}$$

for the coupled GW-plasma system. Here, the parameter g is given by $g = \sqrt{2G}B_0/c$, and the sound velocity c_s is defined as $c_s^2 = \partial P/\partial\rho$. Equation (34) can be written

equivalently in the following suitable form:

$$(\omega^2 - \omega_{gw}^2 - g^2)(\omega^2 - \omega_s^2) = \omega_{ms}^2(\omega^2 - \omega_{gw}^2 + g^2), \tag{35}$$

where the characteristic frequencies ω_{gw} (GW frequency), ω_s (sound frequency), and ω_{ms} (magnetosonic frequency) are given by $\omega_{gw} = k_z c$, $\omega_{ms} = k_z u_A$, and $\omega_s = k_z \tilde{c}_s$, respectively. Here, u_A is the relativistic Alfvén velocity, $u_A^2 = v_A^2/[1 + v_A^2/c^2]$, where $v_A^2 = B_0^2/4\pi\{\rho_0 + \Gamma P_0/[(\Gamma - 1)c^2]\}^{-1}$, and $\tilde{c}_s$ is a modified sound velocity given by $\tilde{c}_s^2 = c_s^2 u_A^2(4\pi\rho_0/B_0^2)$.

Solving the dispersion relation Eq. (35) for ω, we find

$$\omega^2 = \frac{\omega_{gw}^2 + \omega_{ms}^2 + g^2 + \omega_s^2 \pm \sqrt{(\omega_{gw}^2 - \omega_{ms}^2)^2 + (g^2 - \omega_s^2)^2 + 2[\omega_{gw}^2(g^2 - \omega_s^2) + \omega_{ms}^2(3g^2 + \omega_s^2)]}}{2}. \tag{36}$$

The oscillation frequency of the coupled GW-plasma system is given in terms of known characteristic frequencies. In the limit of interest here, i.e. close to resonance where B_0 is so large that the relativistic Alfvén speed is almost equal to the speed of light, $u_A \approx c$, so that as a consequence $\omega_{gw} \simeq \omega_{ms} \gg \omega_s, g$, Eq. (36) can be simplified to

$$\omega^2 \simeq \omega_{gw}^2 \pm \sqrt{\frac{5G}{2}}\frac{B_0}{c}\omega_{gw}. \tag{37}$$

It is obvious that only the lower sign of Eq. (37) is physically meaningful. Even in the case of resonance, there exists a small frequency shift [the second term on the right-hand side of Eq. (37)], which depends on the magnetic field strength, and which can be attributed to the coupling terms in the GW-plasma system.

A. The nature of the GW plasma interaction

It is convenient to explain the nature of the GW-plasma interaction in the frame of the linearized equations. The linearized Faraday's equation [Eq. (25)], upon inserting $E_{y,1} = -\frac{1}{c}V_{z,1}B_0$ from the linearized Ohm's law [Eq. (24)], takes the form

$$\partial_t B_{x,1} = -B_0\partial_z V_{z,1} + \tfrac{1}{2}B_0\partial_t h \tag{38}$$

(here and in the following, $E_{y,1}$, $V_{z,1}$, $B_{x,1} \equiv B_x - B_0$, and $q_{z,1}$ are first order quantities). Linearizing the momentum equation [Eq. (26)], we find, on neglecting the thermal pressure,

$$\partial_t q_{\hat{z},1} + \frac{c^2}{8\pi}2B_0\partial_z B_{x,1} + \frac{c^2}{8\pi}B_0^2\partial_z h = 0. \tag{39}$$

The linearized momentum $q_{\hat{z},1}$ [Eq. (27)] is related to the velocity as

$$q_{\hat{z},1} = \rho_0 c^2 V_{z,1} + \frac{1}{4\pi}B_0^2 V_{z,1}, \tag{40}$$

where we have again neglected the pressure. In a tenuous and strongly magnetized plasma, the matter energy density is much smaller than the magnetic energy density, so that $q_{\hat{z},1} \approx \frac{1}{4\pi}B_0^2 V_{z,1}$, and, for a plane GW, the term $(c^2/2)\partial_z h$ equals $-(c/2)\partial_t h$. Inserting into Eq. (39), we find

$$B_0^2\partial_t V_{z,1} + c^2 B_0\partial_z B_{x,1} + \frac{c}{2}B_0^2\partial_t h = 0. \tag{41}$$

The continuity equation (28) contains no first order GW coupling term.

Both the magnetic field equation (38) and the momentum equation (41) contain a GW coupling term proportional to the GW amplitude. Since these coupling terms are also proportional to B_0 or B_0^2, respectively, it is evident that the GW-plasma coupling is the more effective, the stronger the background magnetic field B_0 is, with an upper limit for the efficiency that can be given only through a nonlinear feedback mechanism.

The GW-plasma interaction can then be described as follows: The induction equation, Eq. (38), shows that the GW tries to modulate the magnetic field periodically; it actually continuously compresses and relaxes the magnetic field through the term $\frac{1}{2}B_0\partial_t h$ (see also e.g. [6,20] and the illustrations therein). This modulation acts as an "electromotive force," additional to the one caused by the electric field in the classical Faraday's law ($-B_0\partial_z V_{z,1}$), and it induces a fluctuating magnetic field on top of the background magnetic field. Turning then to the momentum equation, Eq. (41), we first note that for B_0 of the order of 10^{15} Gauss, our numerical results show that the magnetic term $c^2 B_0\partial_z B_{x,1}$ is larger than the GW coupling term ($\frac{c}{2}B_0^2\partial_t h$), so that the fluid is excited mainly through the magnetic field. This magnetic term represents the force exerted by the magnetic pressure on the fluid; fluid modes are thus activated as a reaction to fluctuations in the magnetic pressure {the corresponding pressure term in the nonlinear momentum equation, Eq. (26), is $\partial_z[\frac{c^2}{8\pi}(B_x^2)]$}.

The GW-plasma interaction and its efficiency are thus not mediated through matter, as it would be if electric currents would be excited by the GW, but they are due to the primary and direct coupling of the GW to the magnetic field, by adding a gravitational electromotive force to Faraday's equation. The excitation of fluid oscillations is a secondary effect, caused by magnetic pressure fluctuations, which in turn gives rise to electric field fluctuations according to Ohm's law. Also a secondary effect is the appearance of currents, which in the ideal MHD approach are due to magnetic field inhomogeneities, $\vec{J} = \frac{c}{4\pi}\nabla \times \vec{B}$. We just note that the GW is not able to directly generate currents through charge separation, since it is insensitive to the sign of charges.

IV. NUMERICAL SOLUTION

We solve the GW-plasma system of equations applying a pseudospectral method that is based on Chebyshev polynomials (see e.g. [21]). The basic principle is that all the spatially dependent variables are expanded in terms of Chebyshev polynomials, which allows one to calculate the spatial derivatives, so that the original partial differential equations turn into a set of coupled, nonlinear ordinary differential equations. Time stepping is then done with the method of lines, using a fourth order Runge-Kutta method with adaptive step-size control, which allows one to prescribe an internal relative precision and to increase or decrease the internal time step, depending on how well or bad the precision criterion is fulfilled.

The one-dimensional grid along the z-direction consists of 256 grid points and corresponds to a physical domain along the z-axis of length $L = 5.410^7$ cm, if not stated otherwise. The sampling time step Δt is set to $\Delta t = T_{gw}/14$, with $T_{gw} = 1/f_{gw}$ and f_{gw} the GW frequency.

A. Parameters, initial and boundary conditions

We assume a background magnetic field B_0 of 10^{15} G, a background density $\rho_0 = 10^{-14}$ g cm^{-3}, and an adiabatic index $\Gamma = 4/3$. The initial conditions are $B_x(z, 0) = B_0$, $V_z(z, 0) = 0$, $\rho(z, 0) = \rho_0$, and $h(z, 0) = 0$. The GW has as boundary condition at the left end z_L of the box $h(z_L, t) = h_0(t)\cos(k_{gw}z_L - \omega_{gw}t)$, so that a monochromatic plane wave is entering the box. The amplitude h_0 rises within roughly 1 ms from 0 to 10^{-4}, at which value it stays constant for about 3 ms (in most applications presented), where after it decays to 0 again.

At the right edge z_R of the box, we apply nonreflecting boundary conditions to $h(z_R, t)$ (based on the analysis of characteristic modes for hyperbolic systems). B_x, V_z, and ρ have free outflow boundary conditions at both edges of the box, where in a thin layer at the boundaries the actual equations gradually are changed to one-way wave equations that allow only outgoing waves (the use of nonreflecting boundaries in the case of B_x, V_z, and ρ basically yielded the same numerical results, at the expense of computing time, though).

The GW frequency is set to $f_{gw} = 5$ kHz, and the GW dispersion relation is of the form $2\pi f_{gw} = \omega_{gw} = k_{gw}c$, with k_{gw} the wave number of the GW.

B. Numerical results

The total mean energy density $\epsilon_{\rm pl}$ in the plasma at a given time t is numerically determined as

$$\epsilon_{\rm pl}(t) = \left[\frac{1}{8\pi}\int E_y(z, t)^2 dz + \frac{1}{8\pi}\int (B_x(z, t) - B_0)^2 dz + \frac{1}{2}\int \rho(z, t) v_z(z, t)^2 dz\right] \Big/ L, \quad (42)$$

with L the size of the system—note that we subtract the constant background magnetic field B_0 in order to take into account only the energy that is in the wave motion. Figure 1 shows $\epsilon_{\rm pl}(t)$ and the mean energy density $\epsilon_{gw}(t)$ of the GW as a function of time, where

$$\epsilon_{gw}(t) = \frac{c^2}{32\pi G}\omega_{gw}^2 \bar{h}(t)^2, \quad (43)$$

with $\bar{h}(t)$ the mean instantaneous amplitude of the GW oscillation, defined as the root mean square average over the entire simulation box [18],

$$\bar{h}(t) = \sqrt{\int h(z, t)^2 dz / L}. \quad (44)$$

In all applications, the box length L is such that the simulation box contains several wavelengths of the GW (nine for the standard value of L), which accounts for the fact that the GW energy density cannot be defined locally (e.g. [18,19]). Moreover, we note that the concept of gravitational energy is only well defined for asymptotically flat spaces ([19]), so that the GW energy calculated here is an approximate, but also usual estimate for the case of a weak GW with a short wavelength compared to the system size (e.g. [18,19]).

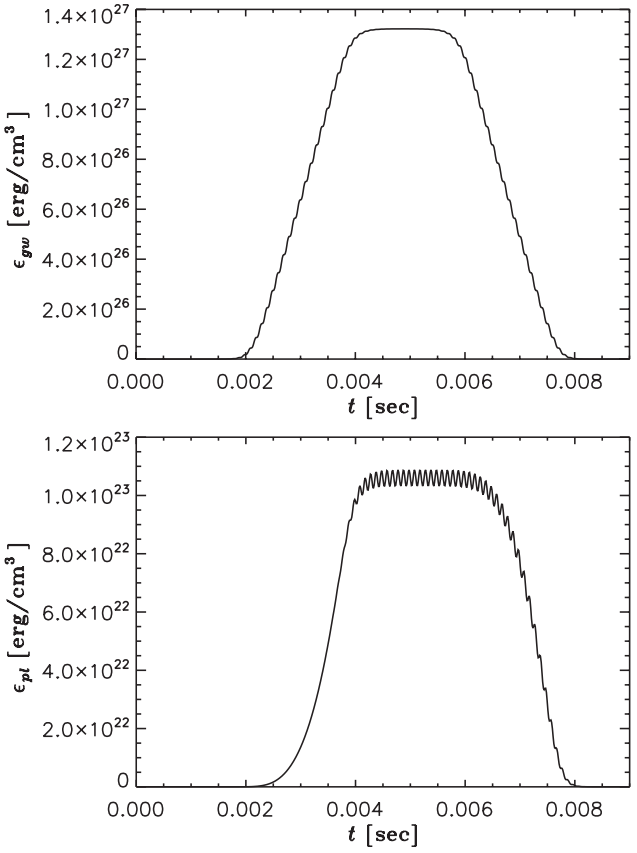

FIG. 1. Top: Average energy density $\epsilon_{gw}(t)$ of the GW as a function of time. Bottom: Mean total energy density $\epsilon_{\rm pl}(t)$ of the plasma as a function of time.

In Fig. 1 then and at maximum GW amplitude, the energy density of the GW amounts to $\epsilon_{gw} = 1.3 \times 10^{27}$ erg/cm^3. Once the GW enters the system, the plasma starts to absorb energy from the GW, and in roughly 2 ms, slightly delayed in the beginning but finally in parallel with the GW reaching its maximum energy, the absorption has reached its maximum, the energy density in the plasma is roughly 10^{23} erg/cm^3. The absorbed energy is a fraction 10^{-4} of the GW energy density, so that the backreaction onto the GW is not yet important. When the GW leaves the system, the energy in the plasma decays almost together with the GW amplitude, i.e. the excited waves propagate out of the simulation box.

The GW excites wave motions in the plasma that travel with the GW and whose amplitudes increase linearly towards the out-flowing edge of the box. Maximum amplitudes attained are 3×10^{12} statvolt/cm (9×10^{16} V/m) for the electric field, 3×10^{12} G for the oscillating magnetic field, roughly 3 orders of magnitude less than B_0, and finally the fluid velocity oscillations have a maximum amplitude 8×10^7 cm/ sec. The fluid motions thus remain nonrelativistic, so that our nonrelativistic estimate of the kinetic energy is justified.

The waves excited in E_y, B_x, and V_z have wave number k_z and frequency ω that cannot be distinguished from k_{gw} and ω_{gw} within the numerical precision of the simulation, see Fig. 2. In particular, we do not find any harmonics to be excited. The relativistic Alfvén speed $u_A^2 = B_0^2/(4\pi\rho_0 + B_0^2/c^2)$ is very close to the speed of light $[(c - u_A)/c = 2 \times 10^{-24}]$ so that the excited plasma modes are indistinguishable from magnetosonic modes.

C. Discussion

The numerical results show that, for strong magnetic fields, a large amount of energy is absorbed by the plasma from the GW on a short time scale, which is of the order of 10 GW periods, i.e. in the millisecond range.

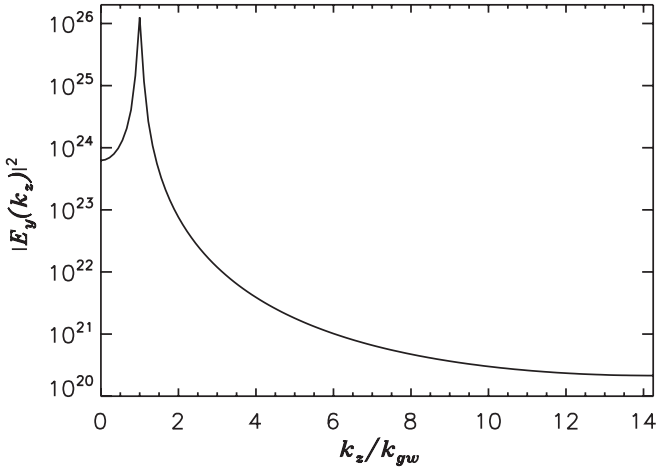

FIG. 2. Spatial Fourier transform $|\hat{E}_y(k_z, t)|^2$ of $E_y(z, t)$ at a fixed time $t = 0.005\,45$ s.

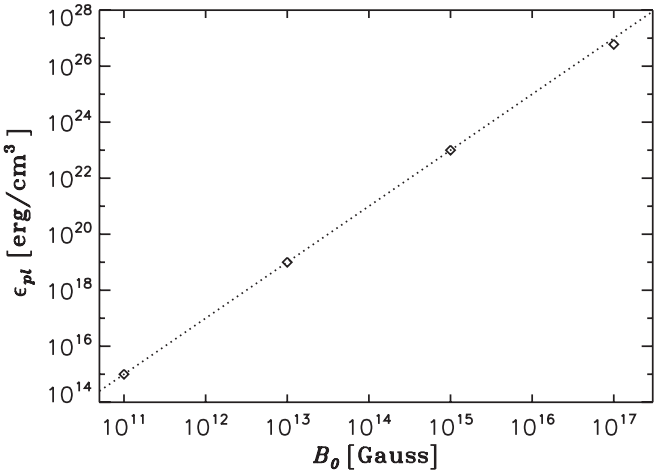

FIG. 3. The energy density $\epsilon_{\rm pl}$ absorbed by the plasma (at maximum absorption) as a function of the background magnetic field B_0 (diamonds), together with a reference line of logarithmic slope 2 (dotted line).

In a parametric study, we found that the energy absorbed by the plasma is proportional to B_0^2 (see Fig. 3) and to h_0^2. Varying ρ_0 in the range 10^{-20} g/cm^3 $\leq \rho_0 \leq 10^5$ g/cm^3, it turned out that the absorbed energy is independent of the value of the matter density ρ_0, see Fig. 4; the kinetic energy is actually negligible compared to the electromagnetic energy (this is in accordance with the fact that the background matter rest-energy density is much smaller than the background magnetic energy density in the entire range of values ρ_0 investigated). The absorbed energy density is furthermore proportional to ω_{gw}^2, as we verified by varying the frequency in the kHz range (from 1 to 10 kHz). It also seems that the time for the plasma needed to reach the maximum level of energy absorption is related to the time needed for the GW to cross the box, L/c, which equals 0.002 sec for the case considered here.

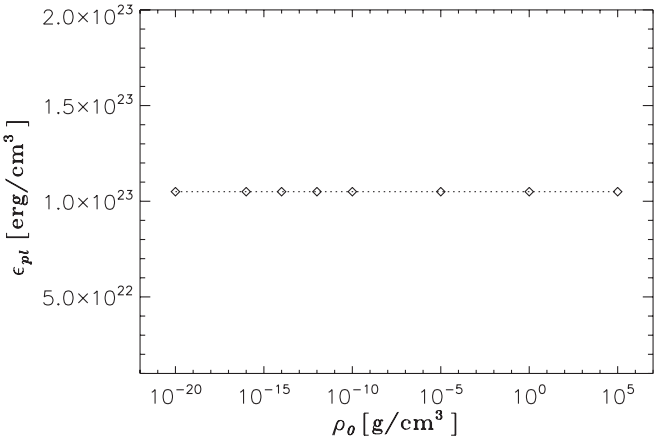

FIG. 4. The energy density $\epsilon_{\rm pl}$ absorbed by the plasma (at maximum absorption) as a function of the background matter density ρ_0 (diamonds, connected with a dotted line).

The maximum amplitudes of the excited oscillations are proportional to the box length L, as explained above. This implies that the amount of energy density absorbed is proportional to the squared box length, L^2, with the physical meaning of L to be the length along the propagation direction of the GW where the GW meets a constant magnetic field. We additionally verified this scaling behavior with numerical simulations in which the box length L was varied. The absorbed energy is thus proportional to L^3 and to the effective area $A_{\rm eff}$ through which the GW is incident on the plasma, where $A_{\rm eff} := V/L$, with V the volume in which the interaction takes place. We can summarize our numerical findings for the total energy $E_{\rm pl}$ absorbed by the plasma as follows, noting that in the case presented here the absorbed energy through an effective area of $1\ {\rm cm}^2$ is $L \times 10^{23}$ erg, with $L = 5.4 \times 10^7$ cm:

$$E_{\rm pl} = 3.4 \times 10^7 \left(\frac{L}{1\ {\rm cm}}\right)^3 \left(\frac{A_{\rm eff}}{1\ {\rm cm}^2}\right) \left(\frac{B_0}{10^{15}\ {\rm G}}\right)^2 \left(\frac{h_0}{10^{-4}}\right)^2 \times \left(\frac{f_{gw}}{5\ {\rm kHz}}\right)^2 {\rm erg}, \quad (45)$$

and $E_{\rm pl}$ is independent of ρ_0.

V. SPHERICAL COORDINATES: DECAYING MAGNETIC FIELD

In applications to spatially extended astrophysical systems, the constancy of the background magnetic field is a strong idealization. Since our scope is to elucidate the response of the plasma to a passing GW, the initial plasma state should be a natural state of the plasma, preferably an MHD equilibrium. In 1D Cartesian systems, nonconstant magnetic fields lead to unstable plasma states, the initial difference in magnetic pressure along the z-direction gives rise to immediate and violent plasma dynamics that aim at flattening the gradient in the magnetic field. Trying to compensate the gradient in magnetic pressure with the plasma pressure, we find, first, that the plasma pressure would have to take unphysically high values, and, second, such setups are still numerically unstable.

We thus proceed in this section to transform the system of equations to spherical coordinates, which will allow one to have decaying magnetic fields as equilibrium initial states for the plasma. The GW is assumed to travel radially outwards, so that in the TT (transverse traceless) gauge and in a *flat orthonormal* spherical frame $(c\hat{t}, \hat{r}, \hat{\theta}, \hat{\varphi})$ the distortion to the flat ONF metric $\eta_{\hat{\alpha}\hat{\beta}}$ caused by the GW is of the form $h_{\hat{\alpha}\hat{\beta}} = {\rm diag}(0, 0, +h(r,t), -h(r,t))$, assuming again a + polarized GW traveling in the $\hat{r}$ direction and oscillating in the perpendicular, $\hat{\theta}$-$\hat{\varphi}$ plane (see [22]; Greek indices in the following refer to the spherical coordinate or ON frame). In the spherical coordinate base (ct, r, θ, φ), the metric then takes the form

$$g_{\alpha\beta} = {\rm diag}(-1, 1, r^2(1+h), r^2\sin^2(\theta)(1-h)). \quad (46)$$

The transformation matrix between the spherical GW coordinate system of Eq. (46) and the corresponding ONF is given by

$$(\mathbf{e}_{\hat{\alpha}})^{\hat{\beta}} = {\rm diag}\left(1, 1, \frac{1}{r\sqrt{1+h}}, \frac{1}{r\sin(\theta)\sqrt{1-h}}\right) \quad (47)$$

and its inverse $(\mathbf{e}^{\hat{\alpha}})_{\hat{\beta}}$.

To construct the Faraday and the fluid stress energy tensor, we can proceed as in the Cartesian case, i.e. we simply write the tensors in the ONF in flat spacetime form, using the observable 3-vector components of $\vec{B}^{(\rm sph)} = (B_r, B_\theta, B_\varphi)$, $\vec{E}^{(\rm sph)} = (E_r, E_\theta, E_\varphi)$, and $\vec{V}^{(\rm sph)} = (V_r, V_\theta, V_\varphi)$. In this way, we have for the Faraday tensor

$$F^{\hat{\alpha}\hat{\beta}} = \begin{pmatrix} 0 & E_r & E_\theta & E_\varphi \\ -E_r & 0 & B_\varphi & -B_\theta \\ -E_\theta & -B_\varphi & 0 & B_r \\ -E_\varphi & B_\theta & -B_r & 0 \end{pmatrix}. \quad (48)$$

(Formally, one simply has to replace the indices as $x \rightarrow r$, $y \rightarrow \theta$, $z \rightarrow \varphi$ in the Cartesian flat spacetime form, as can be verified by the explicit procedure of first formulating the respective tensors in Cartesian, flat spacetime form in terms of $\vec{B}$, $\vec{E}$, and $\vec{V}$, making then a coordinate transformation to flat spherical coordinates, identifying the spherical vector components of $\vec{B}^{(\rm sph)}$, $\vec{E}^{(\rm sph)}$, and $\vec{V}^{(\rm sph)}$ from those of $\vec{B}$, $\vec{E}$, and $\vec{V}$, and then transforming to a flat, spherical ON frame.) The energy momentum tensor in the ONF correspondingly is

$$T^{\hat{\alpha}\hat{\beta}}_{\rm (fl)} = Hu^{\hat{\alpha}}u^{\hat{\beta}} + \eta^{\hat{\alpha}\hat{\beta}}pc^2, \quad (49)$$

with the 4-velocity now taking the form $u^{\hat{\alpha}} = \hat{\gamma}(c, V_r, V_\theta, V_\varphi)$.

The covariant derivatives can be done in two ways: Either in the ONF, with the use of the Ricci rotation coefficients [Eq. (4), calculated now from Eq. (47)], or by first transforming to the coordinate base with the transformation Eq. (47), and then using the Christoffel symbols [calculated from the metric Eq. (46)]. The final equations, expressed in the observable variables (B_θ, E_φ, and V_r, see below), are identical in the two kinds of treatment.

The plasma evolution is determined by Faraday's equation, the momentum equation, and the continuity equation, which are formally equivalent to Eqs. (16), (20), and (21), respectively, just with the indices $\hat{a}$, $\hat{b}$, $\hat{c}$ replaced by $\hat{\alpha}$, $\hat{\beta}$, $\hat{\delta}$.

The model is specified completely analogously to the Cartesian case. We focus on MHD modes that propagate along the radial direction; the magnetic field is assumed to be perpendicular to the propagation direction, $\vec{B}^{(\rm sph)} \parallel \hat{\theta}$, as well as the electric field, $\vec{E}^{(\rm sph)} \parallel \hat{\varphi}$, whereas $\vec{V}^{(\rm sph)} \parallel \hat{r}$. The

nonzero plasma variables are thus B_θ, E_φ, and V_r, and they all spatially depend only on r.

To derive the final equations, we again explicitly expand the covariant derivatives, keeping all nonlinearities, and expressing all components in terms of the observable variables B_θ, E_φ, and V_r. The final equations are found to be formally equivalent to the Cartesian case, in particular, the gravitational coupling terms remain the same, only the partial derivatives are corrected in the way usual for flat spherical coordinates. The reason is that the geometrical setup used is completely equivalent to the one in the Cartesian case, and, of course, the use of spherical coordinates leaves the curvature of spacetime unchanged. After all, the electric field is given from the adjusted Eq. (14) as $E_\varphi = -\frac{1}{c} V_r B_\theta$; Faraday's equation [from the adjusted Eq. (16)] writes

$$\partial_t B_\theta = c\partial_r E_\varphi + cE_\varphi/r + \frac{1}{2} B_\theta \frac{\partial_t h}{1-h} - \frac{1}{2} cE_\varphi \frac{\partial_r h}{1-h}. \tag{50}$$

The r-component of the momentum equation [from the adjusted Eq. (20)] is

$$\begin{aligned}
&\partial_t q_{\hat{r}} + \partial_r \left[\left(q_{\hat{r}} - \frac{c}{4\pi}(-E_\varphi B_\theta) \right) V_r \right] \\
&\quad + \frac{2}{r} \left[\left(q_{\hat{r}} - \frac{c}{4\pi}(-E_\varphi B_\theta) \right) V_r \right] + \partial_r \left[\frac{c^2}{8\pi}(B_\theta^2 + E_\phi^2) \right] \\
&\quad + \frac{2}{r} \left[\frac{c^2}{8\pi}(B_\theta^2 + E_\phi^2) \right] + c^2 \partial_r p + \frac{c}{8\pi} B_\theta (cB_\theta + E_\varphi V_r) \\
&\qquad \times \frac{\partial_r h}{(1+h)} - \frac{c}{8\pi} E_\varphi (cE_\varphi + B_\theta V_r) \frac{\partial_r h}{(1-h)} \\
&\qquad\quad - q_{\hat{z}} (\partial_t h + V_r \partial_r h) \frac{h}{1-h^2} = 0,
\end{aligned} \tag{51}$$

where we defined the new momentum variable $q_{\hat{r}}$ as $q_{\hat{r}} := HV_r \hat{\gamma}^2 + \frac{c}{4\pi}(-E_\varphi B_\theta)$. The continuity equation [from the adjusted Eq. (21)] takes the form

$$\partial_t D + \partial_r (DV_r) + 2DV_r/r - (D\partial_t h + DV_r \partial_r h) \frac{h}{1-h^2} = 0, \tag{52}$$

with the density variable $D := \hat{\gamma}\rho$.

To determine the GW evolution equation in spherical coordinates, we write the Laplacian in Eq. (22) in its usual spherical form, assuming h to be spatially dependent only on r, which yields

$$\partial_{tt} h = c^2 \partial_{rr} h + \frac{2}{r} c^2 \partial_r h. \tag{53}$$

We have omitted the backreaction of the plasma here, since the results in Cartesian coordinates, for which more energy is expected to be absorbed than for the case of decaying background magnetic fields, showed that the backreaction is not important for the range of background magnetic fields B_0 considered here. For numerical purposes, we again have to turn Eq. (53) into a system that is first order in time, defining $a := \partial_t h$, and $b := c\partial_r h$, so that

$$\partial_t h = a \tag{54}$$

$$\partial_t a = c\partial_r b + c2b/r \tag{55}$$

$$\partial_t b = c\partial_r a. \tag{56}$$

The numerical implementation is basically identical to the Cartesian case, including the treatment of the boundaries, just the extra terms of the equations have to be added, and, in the case we use free outflow boundaries, the one-way wave equation has to be replaced by its spherical analogue. The equations are solved in the radial interval $[r_{\rm in}, r_{\rm in} + L]$, with inner boundary $r_{\rm in}$ and radial length L.

A. Numerical results

We assume the background magnetic field to decay spatially as $B_0(r) = B_0(r_{\rm in}/r)$, so that B_0 is the magnetic field at the inner edge $r_{\rm in}$. This falloff corresponds to a natural steady state in spherical coordinates, as can be seen when inserting $B_0(r)$ into Eq. (50) (assuming no GW to be present, $h = 0$). Similarly, we set the background density to $\rho_0(r) = \rho_0(r_{\rm in}/r)^2$, since if there were an outflow with constant velocity, this density falloff forms a stationary state according to Eq. (52). Finally, from Eq. (51), it is obvious that the momentum is in a stationary state if $V_r \equiv 0$, and we consequently choose the initial condition $V_r(r, t = 0) \equiv 0$. The initial conditions for the magnetic field are $B_\theta(r, t = 0) = B_0(r)$, and for the density we choose $\rho(r, t = 0) = \rho_0(r)$. In the numerical studies following below, the standard parameter values are $B_0 = 10^{15}$ Gauss, $\rho_0 = 10^{-14}$ g/cm^3, and $r_{\rm in} = 5 \times 10^6$ cm.

The gravitational wave is again harmonically driven at the inner edge $r_{\rm in}$ of the simulation box, $h(r_{\rm in}, t) = h_0(r_{\rm in}, t) \cos(k_{gw} r_{\rm in} - \omega_{gw} t)$, where the amplitude $h_0(r_{\rm in}, t)$ rises within roughly 1 ms from 0 to h_0, at which value it stays constant, as in the Cartesian case, and we let $h_0 = 10^{-4}$.

Our main concern is the energy absorbed by the plasma. We thus repeat the parametric study of Sec. IV C for the case of the spatially decaying background magnetic field, varying one parameter at a time and keeping the others fixed. We find again that the energy density $\epsilon_{\rm pl}$ absorbed by the plasma scales as

$$\epsilon_{\rm pl} \propto B_0^2 h_0^2 f_{gw}^2, \tag{57}$$

and that it is independent of the background density, roughly for the same range as shown in Sec. IV C. What changes though is the scaling with the box length L, and moreover the energy density depends on the distance $r_{\rm in}$ from the star at which the inner edge of the simulation box is located. As shown in Fig. 5 (top), the scaling with L is of approximate power-law form only for large L. The scaling

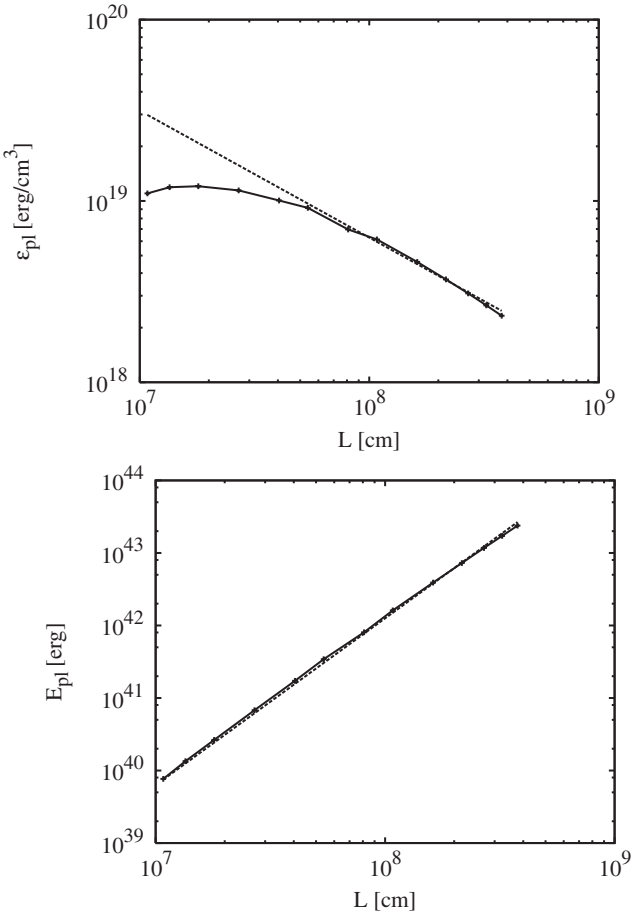

FIG. 5. Top: Mean energy density ϵ_{pl} absorbed by the plasma as a function of box length L, with the inner edge of the simulation box at $r_{in} = 5r_\star$ (plus symbols, connected with solid line), together with a reference line of logarithmic slope -0.7 (dashed line). Bottom: Energy absorbed by the plasma in the conical volume of radial length L and with inner edge at $r_{in} = 5r_\star$ as a function of L (plus symbols, connected with solid line), together with a reference line of logarithmic slope 2.3 (dashed line).

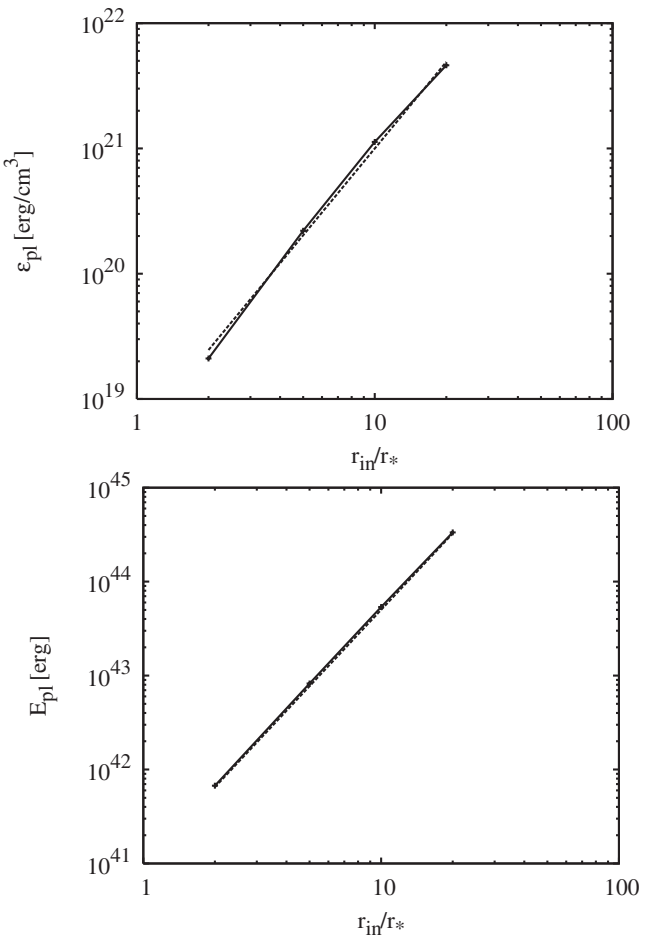

FIG. 6. Top: Mean energy density ϵ_{pl} absorbed by the plasma in the conical volume as a function of the position r_{in} of the inner edge of the simulation box, with fixed box length $L = 540$ km (plus symbols, connected with solid line), together with a reference line of logarithmic slope 2.3 (dashed line). Bottom: Energy absorbed by the plasma in the conical volume of radial length $L = 540$ km, as a function of the position of the inner edge r_{in} of the simulation box (plus symbols, connected with solid line), together with a reference line of logarithmic slope 2.7 (dashed line).

with r_{in} (Fig. 6, top), on the other hand, is of rough power-law form in the entire investigated range. On determining the power-law indices, the energy density is found to exhibit the approximate scaling

$$\epsilon_{pl} \propto r_{in}^{2.3} L^{-0.7} \tag{58}$$

for L large.

In order to get an estimate of the energy absorbed by the plasma, we have to assume a specific geometry for the plasma volume. In view of the scenario of a star with a dipole magnetic field that emits GWs, we focus on the region near the equatorial plane where the GW propagation direction and the magnetic field are perpendicular. We thus consider the plasma in the conical volume of radial size L between the inner and outer radii r_{in} and $r_{out} = r_{in} + L$, respectively (with r the distance from the star), which is limited to within the poloidal opening angle α and the toroidal range φ, as illustrated by the sketch in Fig. 7. The plasma volume is given as

$$V(r_{in}, L) = \tfrac{2}{3}\varphi \sin(\alpha/2)(r_{out}^3 - r_{in}^3), \tag{59}$$

and the total plasma energy E_{pl} in this volume is determined as $E_{pl} = \epsilon_{pl} V(r_{in}, L)$. In the numerical estimates, we assume $\varphi = 180°$ and $\alpha = 10°$. The scaling of E_{pl} with both, L (Fig. 5, bottom), and r_{in} (Fig. 6, bottom), respectively, is of clear power-law form,

$$E_{pl} \propto r_{in}^{2.7} L^{2.3}. \tag{60}$$

In summary then, for the specific plasma volume assumed and on determining the numerical factors, the energy absorbed by the plasma is given by the relation

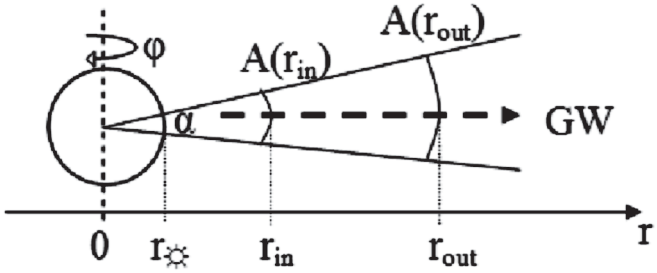

FIG. 7. Sketch: The GW interacts with a plasma volume in the equatorial plane (see text for details).

$$E_{\rm pl} = 1.1 \times 10^7 \left(\frac{r_{\rm in}}{1\ {\rm cm}}\right)^{2.7} \left(\frac{L}{1\ {\rm cm}}\right)^{2.3} \left(\frac{B_0}{10^{15}\ {\rm G}}\right)^2 \left(\frac{h_0}{10^{-4}}\right)^2 \times \left(\frac{f_{gw}}{5\ {\rm kHz}}\right)^2 {\rm erg}, \quad (61)$$

and $E_{\rm pl}$ is independent of ρ_0. Note that in the corresponding Eq. (45) for constant background magnetic field, no assumption on the shape of the volume was made, so that the effective area $A_{\rm eff}$ appears in Eq. (45).

VII. ASTROPHYSICAL APPLICATION AND DISCUSSION

Noteworthy, both equations for the energy, Eq. (45) for constant and Eq. (61) for decaying magnetic field, dimensionally scale with length l as l^5. In Eq. (61), this is immediately obvious from the factor $r_{\rm in}^{2.7} L^{2.3}$, and in Eq. (45) the factor $L^3 A_{\rm eff}$ obviously has dimensions l^5. Equations (45) and (61) are phenomenological equations that summarize the numerical results, and as such we could replace f_{gw}^2 by either k_{gw}^2 or $1/\lambda^2$, using the GW dispersion relation and adjusting of course the numerical factors in the denominator. Remarkably then, Eqs. (45) and (61) would have correct physical units of energy, namely, volume (l^3) times energy density (the units of B_0^2), and the remaining factor of l^2 cancels the units of k_{gw}^2.

Our results imply that the interaction of a GW with a plasma is an efficient mechanism for the energizing of the atmospheres of strongly magnetized stars, most prominently of the atmospheres of magnetars. In the following, we will give an estimate of the mechanism's efficiency.

GWs are expected to be emitted by magnetars, as by usual neutron stars, when they undergo some deformation. There are two distinct kinds of GW emission to be expected, continuous emission as the result of a long lasting deformation of the star, and bursty emission caused by isolated, catastrophic, short duration events (see e.g. [23] for a discussion). Continuous emission allows much weaker GW signals to be detected at the Earth than bursty emission, since the signal can be integrated over an extended observation period. The continuous emission of a compact star typically has a frequency closely related to the spin frequency of the star (e.g. [1]), which for the known magnetars is of the order of several 10^{-1} Hz (e.g. [16,24]). According to both Eqs. (45) and (61), the energy absorption is not very efficient at such low frequencies, so that we do not consider continuous emission here.

Bursty GW emission of magnetars, on the other hand, can be the result of the rearrangement of the strong internal magnetic field (e.g. [25]), or a consequence of crustal cracking (starquake, e.g. [26,27]), caused by stresses exerted on the crust by the strong internal magnetic field. These events have short duration, typically less than a second or even of the order of a few milliseconds (e.g. [23]), and the GW frequency is estimated to lie in the kHz range (e.g. [26]). The GW amplitude near the star is estimated to be of the order 10^{-5} to 10^{-4} (e.g. [25]). For magnetars relatively near to the Earth, the GW signal could in principle be detected; the events are isolated though and have a poor event rate of roughly 10^{-1} events/year, according to [25] (the nearest magnetar known to date is estimated to be at roughly 10 kpc from the Earth, see e.g. [24]).

The magnetic field of neutron stars is poloidal within the light cylinder, so that, near the equatorial plane, a GW generated by the magnetar and traveling radially outwards propagates perpendicular to the magnetic field, as in the presented simulations. The typical magnetic field $B_\star$ of a magnetar is currently estimated to be of the order of 10^{15} to 10^{16} G at the surface (e.g. [13,15,16]), and, as a dipole field, its magnitude falls off as $B_0^{\rm (dip)}(r) = B_\star (r_\star/r)^3$ with distance r from the star. For simplicity, we assume the amplitude of the GW to decay as $h_0^{(gw)}(r) = h_\star (r_\star/r)$, which strictly holds only for large r ($h_\star$ is the GW-amplitude at the stellar surface).

For the energy estimate, we consider the plasma in the conical volume introduced in Sec. [see Eq. (59)] and illustrated by the sketch in Fig. 7, and which is characterized by the inner edge at $r_{\rm in}$ and its radial length L. For the numerical estimates, we set $B_\star = 10^{16}$ G, $h_\star = 10^{-4}$ with GW frequency $f_{gw} = 2$ kHz, $r_\star = 10$ km, $\alpha = 10°$, and, to take possible anisotropic GW emission into account, $\varphi = 180°$.

A. Energy estimate with constant magnetic field

In the first energy estimate, we use the results from the case of constant background magnetic field, Eq. (45), i.e. we assume the magnetic field and the GW amplitude to be constant over the length L of the interaction volume. Since, according to Eq. (45), the energy depends on the squared values of B_0 and h_0, we set $B_0^2 = \langle (B_0^{\rm (dip)}(r))^2 \rangle$ and $h_0^2 = \langle (h_0^{(gw)}(r))^2 \rangle$, respectively, where $\langle \cdots \rangle$ denotes the mean over the radial interval $[r_{\rm in}, r_{\rm in} + L]$. Finally, with the plasma volume given by Eq. (59), we have for the effective area

$$A_{\rm eff} = V(r_{\rm in}, L)/L. \quad (62)$$

Figure 8 (top) shows the absorbed energy as a function of $r_{\rm in}$ for four different values of L. The energy decreases

fast with distance, it roughly is proportional to $1/r_{\rm in}^{5.7}$, so that at $r_{\rm in} = 5r_\star$, the energy has fallen to $E_{\rm pl} = 4 \times 10^{38}$ erg for e.g. $L = 500$ km. Extrapolating our results to regions closer to the star, we find at $r_{\rm in} = 2r_\star$ and again for $L = 500$ km a plasma energy $E_{\rm pl} = 9 \times 10^{40}$ erg ($E_{\rm pl} = 7 \times 10^{41}$ erg for $L = 1000$ km), which is roughly two to three orders of magnitude less than the energy released in giant flares on magnetars (e.g. [13,15,16]). Even closer to the star, at $r_{\rm in} = r_\star$, the energy is of the order of $E_{\rm pl} = 5 \times 10^{42}$ erg ($E_{\rm pl} = 4 \times 10^{43}$ erg for $L = 1000$ km), approaching marginally the energy observed in giant flares, but still one order of magnitude smaller. The energy determined for $r_{\rm in} = r_\star$ is not a completely justified extrapolation, since for consistency with our numerical results, we have to consider the plasma a few stellar radii away from the magnetar, where the background spacetime can be considered flat, we nevertheless can consider the estimate indicative of the actual energy absorbed. For different values of $B_\star$ and $h_\star$, the energy values given here scale according to Eq. (45) in a straightforward way.

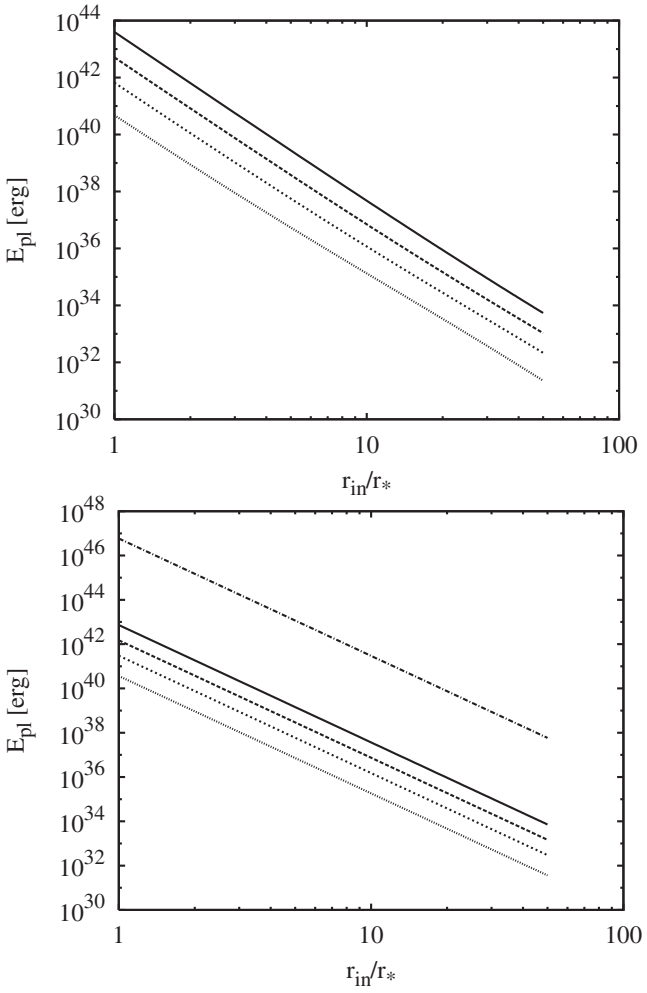

FIG. 8. Top: Estimate of the energy $E_{\rm pl}$ absorbed by the plasma on the base of Eq. (45) as a function of the inner distance $r_{\rm in}$ from the star, for different interaction lengths L (dots: $L = 100$ km; short dashes: $L = 250$ km; long dashes: $L = 500$ km; and solid line: $L = 1000$ km), and for $\alpha = 10°$, $\varphi = 180°$. Bottom: Estimate of the energy $E_{\rm pl}$ absorbed by the plasma as a function of the inner distance $r_{\rm in}$ from the star, on the base of Eq. (61), i.e. for the case of a decaying background magnetic field, and for $L = 5 \times 10^4$ km (dash-dotted line), $L = 1 \times 10^3$ km (solid line), $L = 5 \times 10^2$ km (long dashes), $L = 2.5 \times 10^2$ km (short dashes), and for $L = 1 \times 10^2$ km (dotted line), and for $\alpha = 10°$, $\varphi = 180°$.

For $L = 500$ km, the plasma volume is 2×10^7 km^3 for $r_{\rm in} = r_\star$ and increases to 4×10^7 km^3 for $r_{\rm in} = 10r_\star$, which corresponds to effective areas of $A_{\rm eff} = 5 \times 10^4$ km^2 and $A_{\rm eff} = 8 \times 10^4$ km^2, respectively. The involved volumes and areas are thus relatively small.

B. Energy estimate with decaying magnetic field

The second estimate of the absorbed energy is done using the results from the case of decaying background magnetic field, Eq. (61). Outside the interaction volume, the magnetic field and the GW amplitude are given by $B_0^{(\rm dip)}(r)$ and $h_0^{(gw)}(r)$, respectively. Inside the interaction volume, the magnetic field is assumed to decay as $1/r$, $B_0(r) = B_0(r_{\rm in}/r)$, and we set $B_0 = B_0^{(\rm dip)}(r_{\rm in})$. The magnetic field has thus a realistic decay up to $r_{\rm in}$ and a realistic field strength at $r_{\rm in}$; in the interaction volume it does not decay though fast enough. The GW amplitude, as solution of the spherical wave equation, exhibits a realistic ($\propto 1/r$) falloff also within the interaction region.

The absorbed energy as a function of $r_{\rm in}$ is shown in Fig. 8 (bottom) for different values of L. It falls off as $1/r_{\rm in}^{5.3}$, i.e. less steep than in the case of constant background magnetic field. For the same interaction lengths L as in the case of constant background magnetic field, the energy at $r_{\rm in} = 5r_\star$ is found to be roughly 30% (or, at $r_{\rm in} = r_\star$, one-fourth) of that found in the energy estimate based on constant background magnetic field. In the region of interest relatively close to the star, this second energy estimate yields thus slightly less energy than the first one.

If the magnetic field in the simulation box would decay as $1/r^3$, we would not have to use arbitrary and relatively small values for L, and we could consider the plasma to extend to its physical limit, which is either the light cylinder or the length induced from the GW burst duration. The known magnetars have periods $P_\star$ of the order of seconds (e.g. [16,24]), so that the radius l_{lc} of the light cylinder typically is $l_{\rm lc} = P_\star c/(2\pi) \approx 5 \times 10^4$ km. This distance corresponds to a GW burst duration of 0.2 sec. When setting $L = l_{lc}$, the energy estimate can be considered as a true upper limit for the energy expected to be absorbed in the case of a realistic decay of the magnetic field.

The dash-dotted line in Fig. 8 represents the case $L = l_{lc}$. At $r_{\rm in} = 5r_\star$, the energy in the plasma is $E_{\rm pl} = 1 \times 10^{43}$ erg, which is still less than the energy observed in giant flares, at $r_{\rm in} = 2r_\star$, the energy reaches values of the

order $E_{\rm pl} = 2 \times 10^{45}$ erg, which is a typical energy of giant flares, and finally $E_{\rm pl} = 6 \times 10^{46}$ erg at $r_{\rm in} = r_\star$, which corresponds to the energy observed in the most energetic giant flares, and which, by almost 2 orders of magnitude, is less than the energy that is typically released in a short GRB, according to latest estimates (e.g. [14,16]). With $L = l_{lc}$, the plasma volume is now larger, it amounts to 210^{13} km^3 for $r_{\rm in} = 5r_\star$.

C. Discussion

In both kinds of energy estimate, we assume a realistic falloff of the background magnetic field and the GW amplitude outside the interaction volume. In the interaction volume, we had to make the assumption of either constant background magnetic field and GW amplitude in the first energy estimate, or, in the second energy estimate, realistic decay of the GW amplitude ($\propto 1/r$, not imposed, though, but as it naturally appears as the solution of the spherical wave equation) together with a not steep enough decay of the background magnetic field ($\propto 1/r$ instead of $\propto 1/r^3$). In both energy estimates, the assumed length of the interaction volume is an arbitrary free parameter, except for the one case of the decaying magnetic field where L is set equal to the physical limit, the light cylinder radius. In this case, the corresponding energy estimate can be considered as a true upper limit for the absorbed energy, it is though difficult to estimate how close it is as an approximation.

After all, with the assumptions made in mind, we can conclude that the GW plasma interaction in the vicinity of magnetars is an important mechanism that can energize the plasma considerably on short time scales, depositing energy of the order of at least 10^{41} erg and may be up to 10^{43} erg in the plasma. Given that close to the star the estimated energies are close to but slightly smaller than those observed in giant flares, only the upper limit derived is of the order of the energy seen in the strongest giant flares, we conclude that the GW-plasma interaction mechanism can be the primary energizing mechanism behind giant flares only if, exceptionally, more favoring conditions are met than those assumed here, such as a higher GW frequency, a stronger GW amplitude, a deviation from the $1/r^3$ decay of the background magnetic field, etc. We thus cannot exclude that the GW-plasma interaction is the basic mechanism behind giant flares, the energies we find are though not in favor of such a model. That the GW-plasma interaction is also the primary mechanism behind short GRBs is unlikely on the basis of our results, even the upper limit for the absorbed energy is a few orders of magnitude too small.

Our numerical simulations were done for the case of a flat background spacetime, which does not hold in the range $r_{\rm in} \leq 2r_\star$ anymore, to which we have extrapolated the energy estimates. The nonflatness of spacetime close to the star, together with the main idealizing assumptions as stated above (the necessarily arbitrary choice of a value for L, either the constant magnetic field or the decaying magnetic field with a not steep enough falloff) imply that our energy estimates must be interpreted with some care; they can be taken though as indicative of the fact that the GW-plasma interaction is efficient and is an important mechanism near the star. Also worth mentioning is the uncertainty concerning the actual magnetic topology in the flaring magnetosphere—e.g. the superstrong magnetic field that produces giant flares cannot always be in perfect dipole form—since any deviation from the dipole is likely to intensify the GW-plasma interaction through the enlargement of the possible interaction regions. It thus remains to be seen how far the given numbers will be modified when a more realistic decay ($1/r^3$) of the background magnetic field is used in the simulations and when the curvature of the background spacetime is included. In favor of the model of giant flares on magnetars driven by GWs is that the mechanism has a fast enough time scale, of the order of milliseconds.

VII. CONCLUSION

We derived the equations for the GW-plasma interaction and solved them numerically for the two cases of constant background magnetic field in Cartesian coordinates and radially decaying background magnetic field in spherical coordinates, respectively.

Our results show that strongly magnetized plasmas, with magnetic fields of the order of 10^{15} Gauss, are efficient absorbers of GW energy, largely irrespective of the plasma density, and with an absorption time scale of the order of milliseconds. The results concerning the plasma energetics are summarized in the scaling laws of Eq. (45) for the case of constant background magnetic field, and of Eq. (61) for a decaying background magnetic field, and they imply that GWs may be the energy source for secondary, very energetic phenomena.

The excited plasma modes are of the magnetosonic type, with phase velocity that numerically is indiscernible from the speed of light, and no harmonics are found to be excited. The damping of the GWs is still relatively weak, even for the very strong magnetic fields considered here.

In particular, we can conclude that the GW-plasma interaction is an efficient and important mechanism in magnetar atmospheres, most prominently close to the star. Whether it even is the primary mechanism behind giant flares cannot be excluded on the basis of our results; further investigations are needed though to clear this question.

ACKNOWLEDGMENTS

This work was supported by the Greek Ministry of Education through the PYTHAGORAS program. We thank K. Kokkotas, J. Moortgat, D. Papadopoulos, N. Stergioulas, and J. Ventura for helpful discussions.

[1] K. D. Kokkotas, Classical Quantum Gravity **21**, S501 (2004).
[2] G. Brodin and M. Marklund, Phys. Rev. Lett. **82**, 3012 (1999).
[3] G. Brodin, M. Marklund, and P. K. S. Dunsby, Phys. Rev. D **62**, 104008 (2000).
[4] Yu. G. Ignat'ev, Gravitation Cosmol. **1**, 287 (1995).
[5] A. Källberg, G. Brodin, and M. Bradley, Phys. Rev. D **70**, 044014 (2004).
[6] J. Moortgat and J. Kuijpers, Astron. Astrophys. **402**, 905 (2003).
[7] J. Moortgat and J. Kuijpers, Phys. Rev. D **70**, 023001 (2004).
[8] D. Papadopoulos, N. Stergioulas, L. Vlahos, and J. Kuijpers, Astron. Astrophys. **377**, 701 (2001).
[9] M. Servin and G. Brodin, Phys. Rev. D **68**, 044017 (2003).
[10] M. Servin, G. Brodin, M. Bradley, and M. Marklund, Phys. Rev. E **62**, 8493 (2000).
[11] M. D. Duez, Y. T. Liu, S. L. Shapiro, and B. S. Stephens, Phys. Rev. D **72**, 024028 (2005).
[12] R. C. Duncan and C. Thompson, Astrophys. J. **392**, L9 (1992).
[13] L. Stella, S. Dall'Osso, and G. L. Israel, Astrophys. J. **634**, L165 (2005).
[14] T. Piran, Rev. Mod. Phys. **76**, 1143 (2005).
[15] K. Hurley *et al.*, Nature (London) **434**, 1098 (2005)
[16] E. Nakar, A. Gal-Yam, T. Piran, and D. B. Fox, Astrophys. J. **640**, 849 (2006).
[17] S. J. Schwartz *et al.*, Astrophys. J. **627**, L129 (2005).
[18] J. B. Hartle, *Gravity* (Addison-Wesley, San Francisco, 2003).
[19] L. D. Landau and E. M. Lifshitz, *The Classical Theory of Fields* (Oxford University, New York, 1984), 4th ed.
[20] J. Moortgat and J. Kuijpers, Mon. Not. R. Astron. Soc. **368**, 1110 (2006).
[21] B. Fornberg, *A Practical Guide to Pseudospectral Methods* (Cambridge University Press, Cambridge, England, 1998).
[22] K. S. Thorne and R. D. Blandford, *Applications of Classical Physics* (2004), Chap. 26, http://www.pma.caltech.edu/Courses/ph136/yr2004/.
[23] F. Dubath, F. Foffa, M. A. Gasparini, M. Maggiore, and R. Sturani, Phys. Rev. D **71**, 124003 (2005).
[24] P. M. Woods and C. Thompson, astro-ph/0406133.
[25] K. Ioka, Mon. Not. R. Astron. Soc. **327**, 639 (2001).
[26] E. Coccia, F. Dubath, and M. Maggiore, Phys. Rev. D **70**, 084010 (2004).
[27] J. A. de Freitas Pacheco, Astron. Astrophys. **336**, 397 (1998).